Acta of Bioengineering and Biomechanics
Vol. 18, No. 1, 2016

Original paper
DOI: 10.5277/ABB-00248-2014-02

Biomechanical simulation of needle insertion into cornea based on distortion energy failure criterion

PENG SU, YANG YANG*, LEIYU ZHANG, LONG HUANG

Department of Mechanical Design and Automation, BeiHang University, Beijing, China.

Purpose: This paper is mainly about biomechanical behavior of needle insertion into cornea, and proposes a failure criterion to simulate the insertion process which has attracted considerable attention due to its importance for the minimally invasive treatment. *Methods*: In the process of needle insertion into cornea, tiny and complex insertion force is generated due to contact between needle and soft tissue. Based on the distortion energy theory, there is proposed a failure criterion of corneal material that can solve contact problem between rigid body and biological tissue in insertion simulation, where Cauchy stress of corneal material is the key to numerical calculation. A finite element model of in vivo cornea is built, and the cornea constrained by sclera is simplified to two layers containing epithelium and stroma. Considering the hyper-viscoelastic property of corneal material, insertion simulation is carried out. *Results*: By insertion experiment, the insertion force increases with insertion depth accompanying obvious fluctuations. Different insertion forces are generated at different speeds. The punctured locations are obvious in the force-displacement curves. The results of insertion simulation are generally consistent with experimental data. Maps of von Mises stress reflect the tissue injury of the cornea during insertion process, and punctured status corresponds to the point in the curves. *Conclusions*: The ability of this study to reproduce the behavior of needle insertion into cornea opens a promising perspective for the control of robotic surgery operation as well as the real-time simulation of corneal suture surgery.

Key words: *cornea, biomechanics, insertion force, suture, mathematical simulation*

1. Introduction

The first step of suture surgery operation is the needle insertion into soft tissue. Currently, physicians rely solely on tactile perception and tissue surface distortion to determine the progress of surgical sutures. The judgement is subjective and cannot be used to control the robot-assisted surgery. Because there are many difficulties in the analysis of the internal action of needle insertion into biological tissue, including deformation, relaxation, and parameter settings in mathematical simulation, etc., biomechanical study about the needle insertion into soft tissue has become a bottleneck in the intersection of medicine and mechanics, and it is also a major constraint of robotics development in the medical fields.

Many scholars explored the biomechanics of needle insertion into soft tissue, and pointed out that insertion force could be used for identifying tissue layers as needle inserted into tissues [1]. Naturally, needle deflection and tissue deformation are major problems for accurate needle insertion. Roesthuis et al. [23] considered the needle to be a cantilever beam supported by springs which have needle-tissue interaction stiffness during an insertion. Van Gerwen et al. [27] proposed a law where insertion forces were affected by numerous factors, such as needle type, insertion speed, and tissue characteristics. Davis et al. [7] experimentally measured and theoretically modeled the force required to insert microneedles into living skin and the force needles can withstand before fracturing, and the results provide the ability to predict insertion and fracture forces. Although the cornea has different mechanical properties, insertion theories and

* Corresponding author: Yang Yang, School of Mechanical Engineering and Automation, Beihang University, XueYuan Road No. 37, Hai Dian District, Beijing 100191, China. Phone number: +86 01082338386, e-mail: yang_mech@126.com

Received: December 5th, 2014
Accepted for publication: April 14th, 2015

modeling methods of these studies can serve as a useful reference for biomechanical study of needle insertion into cornea.

The insertion force distribution may be used for real-time simulations of graphic location and tactile feedback, and the numerical simulation can become a valuable tool to plan ophthalmo-surgical procedures [25]. Marshall et al. [20] presented a suturing simulator for surgery operating on spring-mass surface meshes, and when the needle pierced the deformable model, the surface mesh was subdivided at the contact point using a novel subdivision algorithm. Di Maio et al. [8] developed a two-dimensional linear elastostatic material model to quantify the needle forces and soft tissue deformations. Similarly, Berkley et al. [4] have developed a contact mechanism that applies constraints to linear elastic models, and it emphasizes high model resolution, multipoint contact, rapid preprocessing, etc.

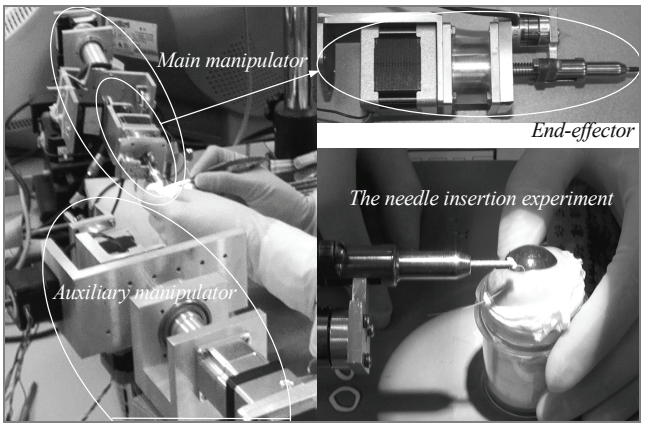

Fig. 1. The cornea-suturing robot. An end-effector with needle mounted on the main manipulator, and the first step is the needle inserts into cornea in the corneal suture [30], [31]

Currently, most of the insertion studies focused on skin and internal organs, while the study is much less in the field of corneal microsurgery that requires more accuracy and precision. In the previous study, we have designed a cornea-suturing robot that has a main manipulator and an auxiliary manipulator, as shown in Fig. 1. By comparing with the conventional manual surgery, we found that robotic suturing has some advantages: more stable suturing, smaller distortion torque and fewer invasions to tissues [30], [31]. There were some key points that affected the success in conducting robot-assisted microsurgical suture, for example, the motion path of robot-end. If using the traditional displacement control, the needle might cause tissue damage due to a lack of force feedback from robot-end. However, surgery would be safer if the robot were controlled by references to the needle force [1], [31]. Therefore, the study objective of this paper is to research biomechanical behavior of needle insertion into cornea that is an efficient reference to ensure the success of robot-assisted surgery, and verify insertion modeling because it is one of the key technologies to simulate the process of corneal surgery.

This paper proposes a distortion energy failure criterion of corneal material in insertion simulation, and the element will lose carrying capacity if the condition of yield failure is met. Then insertion experimentation and simulation have been done to verify the failure criterion. In the simulation, corneal material properties are accurately described by a hyper-viscoelastic corneal model deduced in the previous study [26], and a finite element model of the cornea simplified to two layers containing epithelium and stroma is built. Mesh elements of the insertion contact area are locally refined in the finite element analysis to adapt to the distribution characteristics of calculation data. The results show that the failure criterion proposed is effective in insertion simulation by comparisons with the relationships between the insertion force and depth in experiment.

2. Materials and methods

2.1. Biological structure and material behavior

The cornea has the macroscopic structure of a thin shell in front wall of the eye. Assuming corneal surface is substantially spherical, it has a different thickness at each position, and pupillary zone is the thinnest. In this paper, porcine cornea is taken as the research object, and geometric parameters of the cornea are shown in Table 1 [2], [9], [24].

Table 1. Corneal geometric parameters (mm) [2], [9], [24]

Parameter	Value	Parameter	Value
Axial length	26.50	Horizontal diameter	11.20
Corneal mean thickness	0.67	vertical diameter	11.00
Central thickness	0.55	Pericentral thickness	0.72
Peripheral thickness	1.00	Corneal anterior radius	7.80
Corneal posterior radius	6.80		

At the micro level, the cornea is mainly composed of collagen fibrils embedded within a matrix of proteoglycans, and this construction leads to difficulties

in understanding the material behaviour. The cornea can be divided into five layers, including epithelium, lamina elastica anterior, stroma, lamina elastica posterior, and endothelium, as seen in Fig. 2 [3], wherein, stroma is the main load-bearing part, accounting for about 90% of the corneal thickness. The biomechanical properties of the cornea are primarily derived from the stroma [16]. Epithelium, located outermost layer of cornea, is generally considered to be a corneal barrier that is harder than the other layers, but it is only a small contribution to the corneal tensile strength as it hardly bears the loads [13]. Lamina elastica anterior has no actually elasticity, which serves as the basis of the epithelium, and some scholars believe that it has lower contribution to the biomechanical properties of cornea [9]. Lamina elastica posterior is a transparent film that is flexible and resistant, and it can buffer the effect of IOP (i.e., Intra-ocular pressure) for cornea. Endothelium also hardly bears the load whose density is consistent with epithelium.

Normally cornea is in a tensioned state, and it is difficult to quantitatively describe the corneal biomechanical properties because there are many factors that can affect them, e.g., age, gender, and IOP, etc., [10], [11], [19] Besides, in the original data reported by different authors, some differences between the sets of test results are observed because of different testing conditions or testing protocols [26]. Naturally, the results are consistent as to the scope and trend.

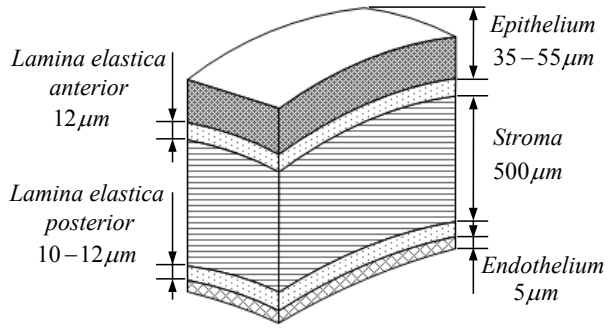

Fig. 2. Corneal micro-structure diagram [3]

Corneal material has two significant characteristics: hyperelastic and viscoelastic, and we have developed a corneal model in the previous study [26]. Firstly, the Mooney–Rivlin hyperelastic model of cornea obtained based on stored-energy function can be simplified as a linear equation with two unknown parameters. Then, modified Maxwell viscoelastic model of the cornea whose analytical form is consistent with the generalized Prony-series model is proposed from the perspective of material mechanics. Parameters of the model are determined by the uniaxial tensile tests and the stress-relaxation tests.

The Mooney–Rivlin hyperelastic constitutive model of the cornea may be described as

$$W = 10.59 \cdot (\bar{I}_1 - 3) - 11.20 \cdot (\bar{I}_2 - 3), \qquad (1)$$

where $\bar{I}_1 = J^{-\frac{2}{3}} I_1$ and $\bar{I}_2 = J^{-\frac{4}{3}} I_2$ represent the first and second invariant of isochoric part $\overline{C}$ of the right Cauchy–Green deformation tensor C. The expansion ratio $J = I_3^{\frac{1}{2}}$ represents volume ratio of deformation. I_1, I_2, and I_3 are three basic invariants of tensor C.

The modified Maxwell viscoelastic model of the cornea may be described as

$$G(t) = \sum_{i=1}^{4} E_i e^{-t/\tau} + E_5, \qquad (2)$$

where E_i is relaxation modulus (unit: MPa), and τ_i is relaxation time (unit: s), expressed by

$$(E_1, E_2, E_3, E_4, E_5) = (0.69, 0.43, 0.31, 0.40, 0.43)$$

and

$$(\tau_1, \tau_2, \tau_3, \tau_4) = (8.83, 65.33, 876.93, 2.84 \times 10^3).$$

The hyperelastic model and viscoelastic model of the cornea are established respectively. The hyperelastic property of deformation-recovery and time-dependent viscoelastic property should be considered at the same time under loading conditions. In general, it can be attributed to the non-linear hyper-viscoelastic problem. It is a complex problem in the field of solid mechanics because the relationship between the deformation rate and time rate is a series of energy conversion behavior.

2.2. Finite element model

According to the description above, a model of needle insertion into cornea can be established in ABAQUS, as shown in Fig. 3 (a). Due to a small difference in the properties of the two orthogonal directions, the corneal model simplified as an axisymmetry one is verified by extrusion in vivo cornea [22], [26]. Many researchers have studied the cornea as a whole, but they did not indicate specific structural layer relative to the measured biomechanical parameters. It is necessary to distinguish the structural layer on simulation because the layers of the

cornea may affect the insertion force. Undoubtedly, stroma is essential in a simulation model. Epithelium that is the second thicker layer of the cornea after the stroma has a greater cell density, so it should be considered in simulation model. Finally, other layers are so thin that we ignore their impact on the simulation results. According to Table 1 and Fig. 2, corneal central thickness is 0.55 mm in the model where stroma-thickness is 0.5 mm and epithelium-thickness is assumed to be 0.067 mm.

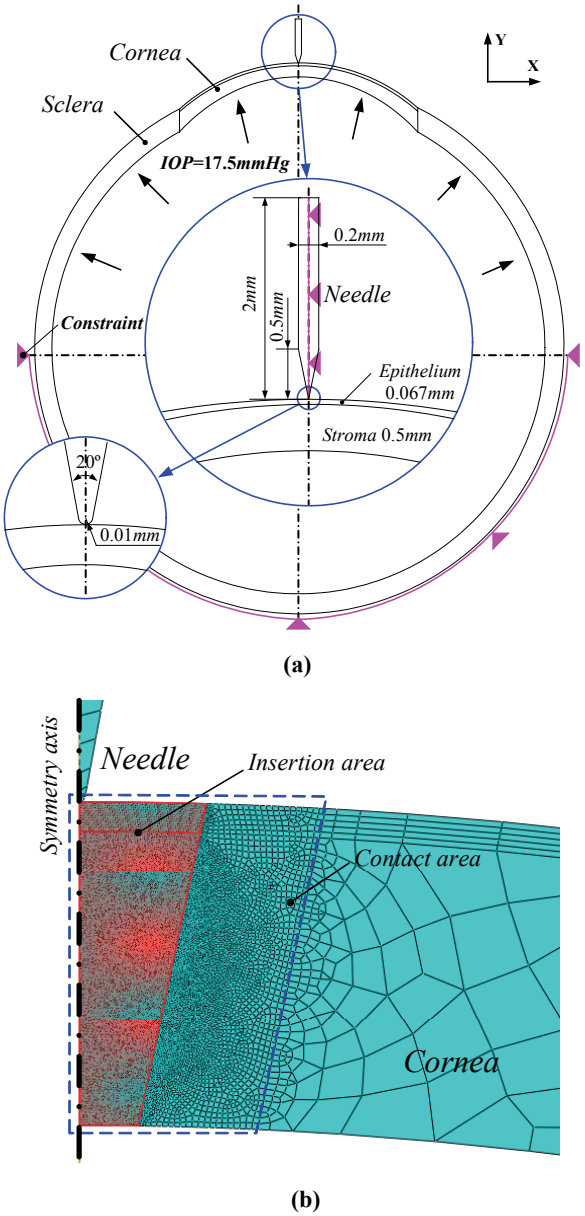

Fig. 3. (a) The model of needle insertion into cornea, (b) meshing of local area

The material model is established based on corneal hyper-viscoelastic parameters above. The destruction intensity of the cornea increases with age [19], so it is difficult to determine a precise value of the failure stress. This paper found the prediction results of numerical simulation were basically in agreement with experimental results when the failure stresses of epithelium and stroma are set to 10 MPa and 5 MPa which are estimates based on corneal biomechanical study of laser in situ keratomileusis (LASIK) [12]. The lower hemisphere of the model is hinged constraints, and the needle, seen as a rigid body, is constrained in the x direction, as shown in Fig. 3 (a). In the previous study, the in vivo model of the cornea is validated by experiment and simulation of extrusion in vivo cornea [26]. Based on the actual state of the eye, the cornea is constrained by sclera which is simplified as an elastomer, and material behaviors of the sclera can be described by elastic modulus E = 3.08 MPa and Poisson's ratio μ = 0.49 [5]. It is an effective way to deal with constraint problem of the cornea. Besides, the value of IOP is 17.5 mmHg (i.e., 2.33×10^{-3} MPa), which is proven effective value by extrusion simulation under different IOP.

Considering factors like computational accuracy, efficiency, displacement coordination, and convergence, etc., the model is divided into 16923 mesh elements, where the element type is CAX4R, a 4-node bilinear axisymmetric quadrilateral in axisymmetric stress family, element controls include reduced integration, distortion control, and enhanced hourglass control. In order to ensure accuracy of the calculation, the meshes of corneal contact area should be refined, wherein the insertion area is divided into 11683 mesh elements that accounts for nearly 70% of total elements in order to adapt to the distribution characteristics of calculation data, as shown in Fig. 3 (b). During insertion, the contact surface between the needle and corneal is changing, so surface-to-surface (explicit) contact is created, where needle is set to be the first surface and contact area is the second surface. Interaction parameters are as follows: mechanical constraint formulation is penalty contact method, sliding formulation is finite sliding, and pressure-over closure normal behavior of the hard-contact. In addition, friction tangential behavior of insertion cornea is related with the viscous of biological tissue, and it will change with insertion speed. Based on the modified Kamopp friction model [21], Xuan et al. have established a friction model through a series of sine loading tests, and when insertion speed $\dot{x} \geq 0.84$ mm/s, the friction can be given by [28]

$$f(\dot{x}) = -0.371\,\mathrm{sgn}(\dot{x}) + 0.1171\dot{x}\,. \tag{3}$$

2.3. The distortion energy failure criterion

In the finite element analysis, a failure criterion should be set to control element deletion. There are three common failure criterions: the maximum principal strain, the maximum principal stress, and von-Mises stress failure criterion. The first two are mainly used for failure analysis of brittle materials [14]. Besides, the von Mises stress criterion is widely used in polymeric materials, such as strength and failure analysis of plastics and rubber [15], [29].

The von Mises stress failure criterion, also known as distortion energy failure criteria, originated in the distortion energy theory (i.e., the fourth strength theory), and it is suitable for small strain. Based on the relationship of stress-strain in the previous study, the mean value of corneal strain in the normal physiological stage is about 0.17 [26]. When the criterion is met, relevant elements of the model are damaged and invalid due to the loss of carrying capacity. In this paper, distortion energy theory was chosen as the failure theory of needle insertion into cornea because of the similar material properties between cornea and other hyperelastic materials.

Firstly, von Mises stress of corneal material should be determined as it is the key to numerical calculation. Constitutive model (1) above may be represented as

$$W = W(\bar{I}_1, \bar{I}_2, J)$$

$$= C_{10}(\bar{I}_1 - 3) + C_{01}(\bar{I}_2 - 3) + \frac{1}{D}(J-1)^2, \qquad (4)$$

where volume ratio $J = \det(F)$, and F is the material deformation gradient tensor (i.e., stretching tensor). $\overline{F} = J^{-\frac{1}{3}}F$ is the modified deformation gradient, and there are three tensors: left Cauchy–Green tensor $B = FF^T$, modified left Cauchy–Green tensor $\overline{B} = \overline{F}\overline{F}^T = J^{-\frac{2}{3}}B$, and modified right Cauchy–Green tensor $\overline{C} = \overline{F}^T\overline{F}$. $\overline{B}$ and $\overline{C}$ have the same characteristic value, and $\bar{I}_1 = J^{-\frac{2}{3}}I_1$ and $\bar{I}_2 = J^{-\frac{4}{3}}I_2$ are invariant tensors of the symmetric modified Cauchy–Green tensor [17]. There are partial derivatives

$$\frac{\partial \bar{I}_1}{\partial \overline{C}} = \mathrm{I}, \quad \frac{\partial \bar{I}_2}{\partial \overline{C}} = J^{-\frac{2}{3}}(I_1\mathrm{I} - C),$$

$$\text{and} \quad \frac{\partial J}{\partial C} = \frac{J}{2}C^{-1}. \qquad (5)$$

According to the above definition, equation (5) can be further described as

$$\frac{\partial \bar{I}_1}{\partial C} = J^{-\frac{2}{3}}\left(\mathrm{I} - \frac{1}{3}I_1C^{-1}\right),$$

$$\frac{\partial \bar{I}_2}{\partial C} = J^{-\frac{4}{3}}(I_1\mathrm{I} - C)\left(\mathrm{I} - \frac{1}{3}I_1C^{-1}\right),$$

$$\text{and} \quad \frac{\partial J}{\partial C} = \frac{J}{2}C^{-1}. \qquad (6)$$

There is a potential energy function W in hyperelastic material, which is the potential energy of the second Piola–Kirchhoff stress tensor S, is given by

$$S = 2\frac{\partial W}{\partial C} = 2\left(\frac{\partial W}{\partial \bar{I}_1}\frac{\partial \bar{I}_1}{\partial \overline{C}} + \frac{\partial W}{\partial \bar{I}_2}\frac{\partial \bar{I}_2}{\partial \overline{C}} + \frac{\partial W}{\partial J}\frac{\partial J}{\partial C}\right). \qquad (7)$$

According to equations (4) and (7), tensor S can be described as

$$S = 2C_{10}J^{-\frac{2}{3}}\left(\mathrm{I} - \frac{1}{3}I_1C^{-1}\right)$$

$$+ 2C_{01}J^{-\frac{4}{3}}\left(\frac{4}{3}I_1I - \frac{1}{3}I_1I_1C^{-1} - C\right)$$

$$+ \frac{2}{D}(J-1)JC^{-1}. \qquad (8)$$

The relationship between von Mises stress σ (i.e., Cauchy stress) and stress S can be expressed by

$$\sigma = \frac{1}{J}FSF^T. \qquad (9)$$

Therefore, the expression of von Mises stress σ is

$$\sigma = \frac{2}{J}C_{10}\left(\overline{B} - \frac{1}{3}TI\right)$$

$$+ \frac{2}{J}C_{01}\left(\frac{4}{3}\overline{B}T - \frac{1}{3}TTI - \overline{B}\overline{B}\right)$$

$$+ \frac{2}{D}(J-1)I, \qquad (10)$$

where T is the matrix trace of tensor C, i.e., $T = \mathrm{trace}(\overline{B})$. The expression (10) is the Cauchy stress that can be applied to the material failure criterion.

Secondly, James Clerk Maxwell and Richard von Mises et al. specified von Mises criterion 100 years ago, and some scholars have described that strain en-

ergy density ρ_ε consisted of volume change energy density ρ_V and distortion energy density ρ_D in the study of mechanics of materials [18]. In the complex stress state, ρ_V and ρ_D are given by

$$\rho_V = \frac{1-2\mu}{6E}(\sigma_1+\sigma_2+\sigma_3)^2,$$

$$\rho_D = \frac{1+\mu}{6E}[(\sigma_1-\sigma_2)^2+(\sigma_2-\sigma_3)^2+(\sigma_3-\sigma_1)^2]. \tag{11}$$

For calculating strain energy, the cornea is simplified as an incompressible elastic material whose material parameters can be described by elastic modulus E = 1.8 MPa and Poisson's ratio μ = 0.49 [6], [10]. The expression of ρ_ε can be rendered in the form

$$\rho_\varepsilon = \frac{1}{2E}[\sigma_1^2+\sigma_2^2+\sigma_3^2-2\mu(\sigma_1\sigma_2+\sigma_2\sigma_3+\sigma_3\sigma_1)]. \tag{12}$$

Distortion energy density is considered as the main factor causing material failure in the distortion energy theory. As long as the distortion energy density ρ_D reaches its limit ρ_D^0, the material is damaged [14],

$$\rho_D^0 = \frac{2(1+\mu)}{6E}([\sigma])^2 \tag{13}$$

where $[\sigma]$ is the limiting stress, i.e., breaking strength, which can be obtained by uniaxial tensile test. The yield limit of material can be expressed as

$$\rho_D = \rho_D^0. \tag{14}$$

Therefore, defining state variable as δ, the yield condition can be expressed as

$$\delta = \sqrt{\frac{1}{2}[(\sigma_1-\sigma_2)^2+(\sigma_2-\sigma_3)^2+(\sigma_3-\sigma_1)^2]} \le [\sigma]. \tag{15}$$

The material failure criterion of the cornea will be defined using VUMAT, one of ABAQUS subroutines, and its implementation flowchart is shown in Fig. 4. In material integration points for each time increment, ABAQUS will call VUMAT to perform the calculations about the material. The type of the variable δ is real before comparing with $[\sigma]$, and then it is defined as a constant to determine the state including Failure and Normal. If $\delta < [\sigma]$ in the calculation, state variable δ is defined as 0 (i.e., δ = 0) that means the material is failure. Otherwise, the material is normal when δ = 1. In the next time increment, the program will calculate the next step if the initial state variable $\delta_0 \neq 0$. The parameters of different nonlinear model can be input from the main program because the interface parameters have been set in VUMAT.

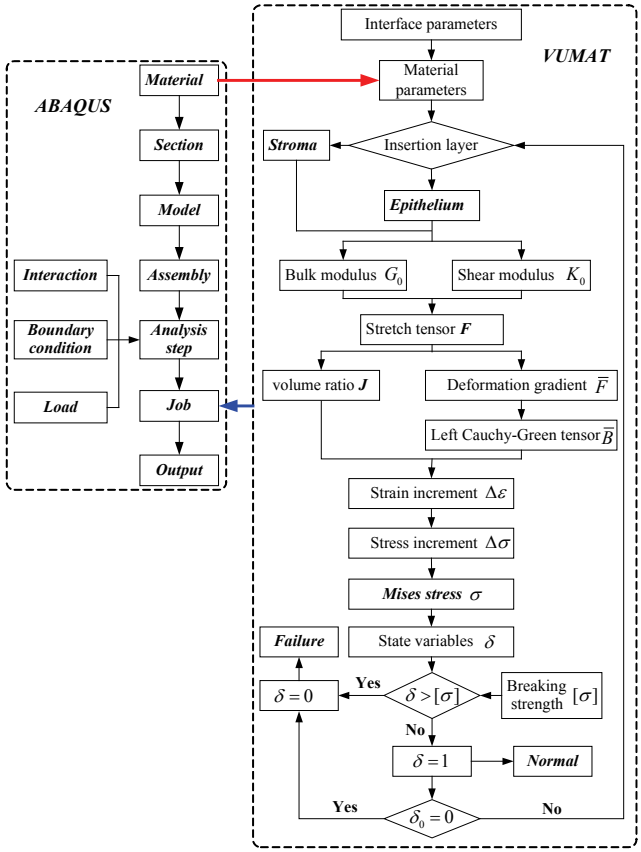

Fig. 4. Implementation flowchart of the distortion energy failure criteria

2.4. Insertion experimentation and simulation

Because cornea is a very complex flexible body, the force is complicated in the process of needle insertion into cornea. The process can be divided into three stages, including contact stage, trajection stage of needle-tip, and trajection stage of needle shaft, as shown in Fig. 5. Firstly, when the needle contacts with the cornea, insertion force is surface contact force, i.e., stiffness force, generated due to the elasticity of tissue before cell units are damaged. After a steady increase, the force reaches a peak value. Secondly, when needle penetrates the top surface of cornea, the insertion force shows sudden drop, and it is constituted of the friction force and cutting force at trajection stage of needle-tip. Finally, when the needle penetrates the underside, entering the trajection stage of needle shaft, the insertion force is mainly constituted by the friction force [1], [21].

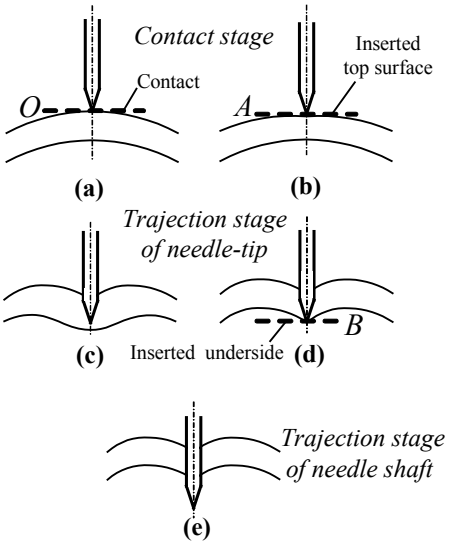

Fig. 5. The process of needle insertion into soft tissue, where *O*, *A*, and *B* are three critical conditions [21]

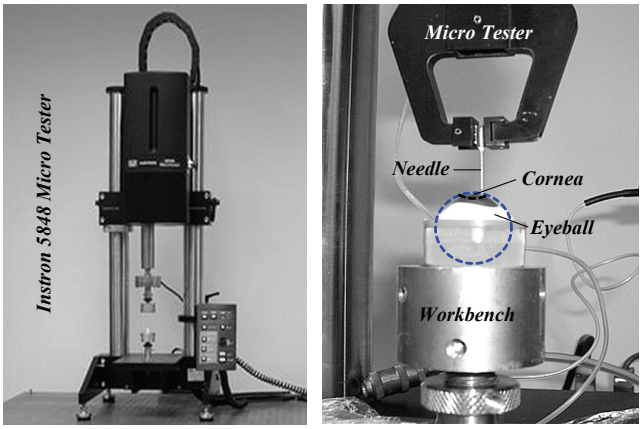

(a) (b)

Fig. 6. (a) Instron 5848 Micro Tester; (b) A experiment of needle insertion into cornea

In order to study the insertion force, and provide a judgment basis for the insertion simulation, experiments of needle insertion into cornea are done using Instron 5848 Micro Tester, as seen in Fig. 6 (a). Considering the accuracy of the data, insertion experiments should be carried out under the same condition that is consistent with the previous experiments on corneal material behavior [26]. The porcine eyes are slaughtered within eight hours. Measurement accuracy of the tester is ±0.4% (load) and ±0.5 μm (displacement). The medical needle No. 2 is selected, 0.2 mm in diameter. In the experiments, the needle is inserted into the cornea at a speed of 1 mm/s or 5 mm/s. In each insertion speed, 10 eyeballs are used and vertical puncture is performed in each eyeball, as shown in Fig. 6 (b). Notably, IOP value of each eyeball is measured with a tonometer in the experiment. The eyeball should be injected with saline to make IOP value reach the ideal value (17.5 mmHg) when the measured value is less. The aim is to maintain the consistency of the internal pressure and remove a cause of experimental variability in the mechanical response.

The process of needle insertion into cornea can be simulated, where the material failure criterion of the cornea is used for all mesh elements. When they reach the failure distortion energy, they lose carrying capacity in the system, and this would be important to the deformation gradient F. The failures of the elements ignore the volume loss that affect volume ratio J. Applying insertion speed 1 mm/s and 5 mm/s at needle-end, the needle is inserted into the cornea, vertically downward along the y-axis. Dynamic explicit step is set, where the simulation time is 0.7 s and the target time increment is 2.0×10^{-5} s.

3. Results

Figure 7 shows insertion force-displacement curve when insertion speed v is 1 m/s, which is obtained by 10 experiments. Analysing the mean value curve, the force shows a stable upward trend with the insertion depth, but there are two relatively distinct inflection points shown as A and B points in the figure. Point A is the puncture of the needle into entire cornea (i.e., the punctured location), where the force will fluctuate significantly if the needle is inserted deeper. Considering the position of point B, some reasons may cause fluctuation of the force such as corneal deformation, tissue friction, etc. Symmetric error bar of standard deviation shows statistical dispersion of 10 experimental data items in the insertion depth, and standard deviation increases with the depth.

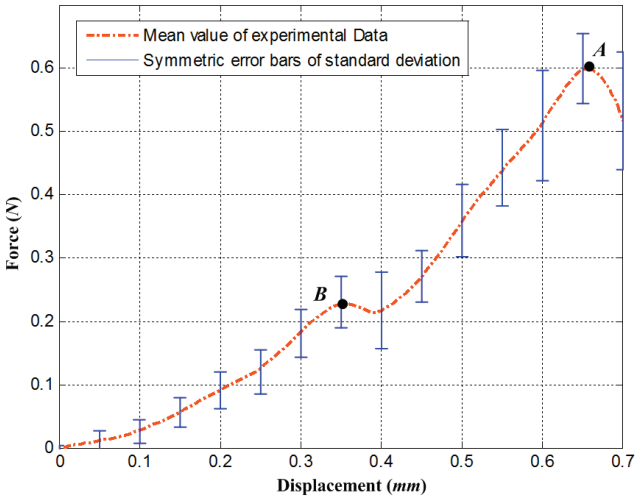

Fig. 7. Experimental data curve of insertion force when insertion speed v is 1 m/s

The force-displacement curves obtained in the simulation are shown as curve *a* and *b* in Fig. 8, where the fitting curve *a* is given by third-order Gaussian interpolation function $F(x)$, shown in equation (15). Usually, the first drop is often used to signal the puncture of the needle into the corneal top layer. The curve *b* is obtained by sample data, i.e., raw simulation result that can reflect small changes for insertion force. So based on curve *b*, points *C* and *D* show epithelium and stroma has been punctured respectively considering the corneal model and corneal deformation. Admittedly, there are some errors between *a* and *c* in Fig. 8 because the reality organisms always have some factors that cannot be simulated, such as local deformation and unequal force. But trend and range of insertion force data are generally the same between simulation and experiment. In addition, experimental result has an obvious hysteresis due to tissue deformation that could lead to more friction. For example, considering the sudden drops of the force on the curves and central thickness of the cornea in Table 1, the punctured position should be at about 0.57 mm (near point *E*), which is smaller than the actual punctured position (point *A*). Undoubtedly, these puncture positions are of major importance when using the simulation for robot-surgery, we can modify these differences according to the similar trend in practice. Statistics on the force of needle insertion into cornea are shown in Table 2, which consists of the mean value of experimental data and fitting value of simulation data at some insertion displacement.

$$F(x)=\sum_{i=1}^{3} a_i \exp\left(-\left(\frac{x-b_i}{c_i}\right)^2\right), \quad x\in[0,0.7] \qquad (16)$$

where

$$\begin{bmatrix} a_1, b_1, c_1 \\ a_2, b_2, c_2 \\ a_3, b_3, c_3 \end{bmatrix} = \begin{bmatrix} 0.46, 0.61, 0.15 \\ 0.40, 0.86, 0.20 \\ 0.22, 0.36, 0.17 \end{bmatrix}.$$

Besides, the comparison plot of different speed is shown in Fig. 9 (b). Comparing the curves at v = 5 mm/s (curves *d* and *e*), the experimental results have significant fluctuations caused by the tissue deformation, and the punctured position in experiment (point *A*) is lagging relative to the simulation position (point *E*). Overall, higher insertion speed tends to increase friction [27] and it is one of the reasons why higher speeds create greater interaction forces in the process. At the larger insertion speed, the fluctuation of simulation force is smaller than experimental force. Obviously, the results of simulation are broadly consistent with experimental data at different speed.

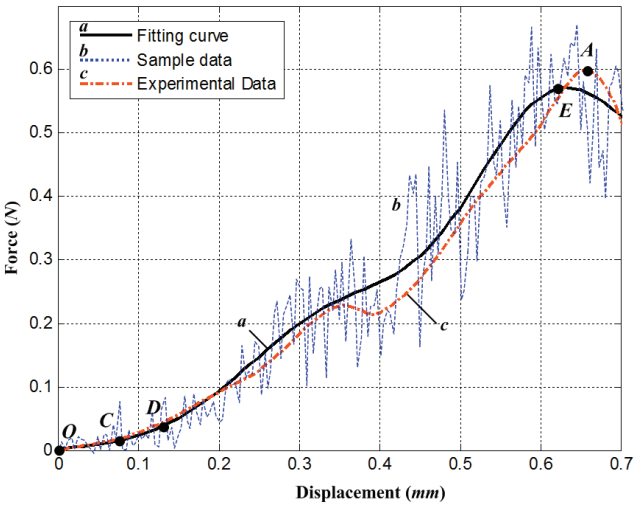

Fig. 8. Insertion force-displacement curves when insertion speed v is 1 mm/s. *a* is the mean value curve of experimental data; *b* is the fitting curve of simulation results by equation (15); *c* is the sample data curve of simulation results

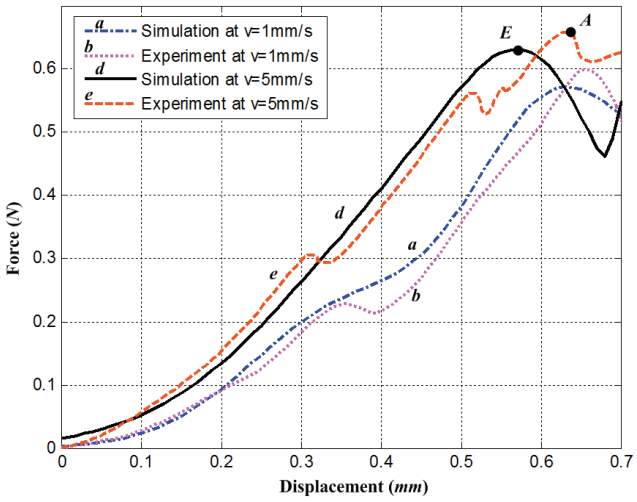

Fig. 9. Insertion force-displacement curves at different insertion speeds. *a* and *b* are the curves shown in Fig. 8; *d* and *e* are the experimental curve and simulation curve when insertion speed v is 5 mm/s

Maps of von Mises stress reflect the tissue injury and deformation of the cornea during insertion process, as shown in Fig. 10, where figures (a), (b), (c), and (e) correspond to points *O*, *C*, *D*, and *E* of Fig. 8, respectively. Wherein, it is clearly seen from figure (c) that the boundary of two layers is due to different failure stresses. In figure (e), it can be considered that the whole cornea was punctured completely. In figure (f), significant elastic deformation occurred at the insertion position, whole cornea, and unconstrained sclera.

Table 2. Statistics on the force of needle insertion into cornea,
where experimental data is the mean value and simulation data is the fitting value

Displacement (mm)	Insertion speed v is 1 m/s		Insertion speed v is 5 m/s	
	Experimental data (N)	Simulation data (N)	Experimental data (N)	Simulation data (N)
0	0	0	0	0.02
0.05	0.01	0.01	0.02	0.03
0.1	0.03	0.02	0.06	0.05
0.15	0.06	0.05	0.10	0.09
0.2	0.09	0.09	0.15	0.13
0.25	0.12	0.15	0.22	0.19
0.3	0.18	0.20	0.30	0.26
0.35	0.24	0.24	0.31	0.34
0.4	0.22	0.26	0.38	0.41
0.45	0.26	0.31	0.15	0.49
0.5	0.36	0.38	0.55	0.57
0.55	0.44	0.48	0.58	0.63
0.6	0.51	0.56	0.64	0.62
0.65	0.62	0.57	0.60	0.53
0.7	0.63	0.53	0.64	0.55

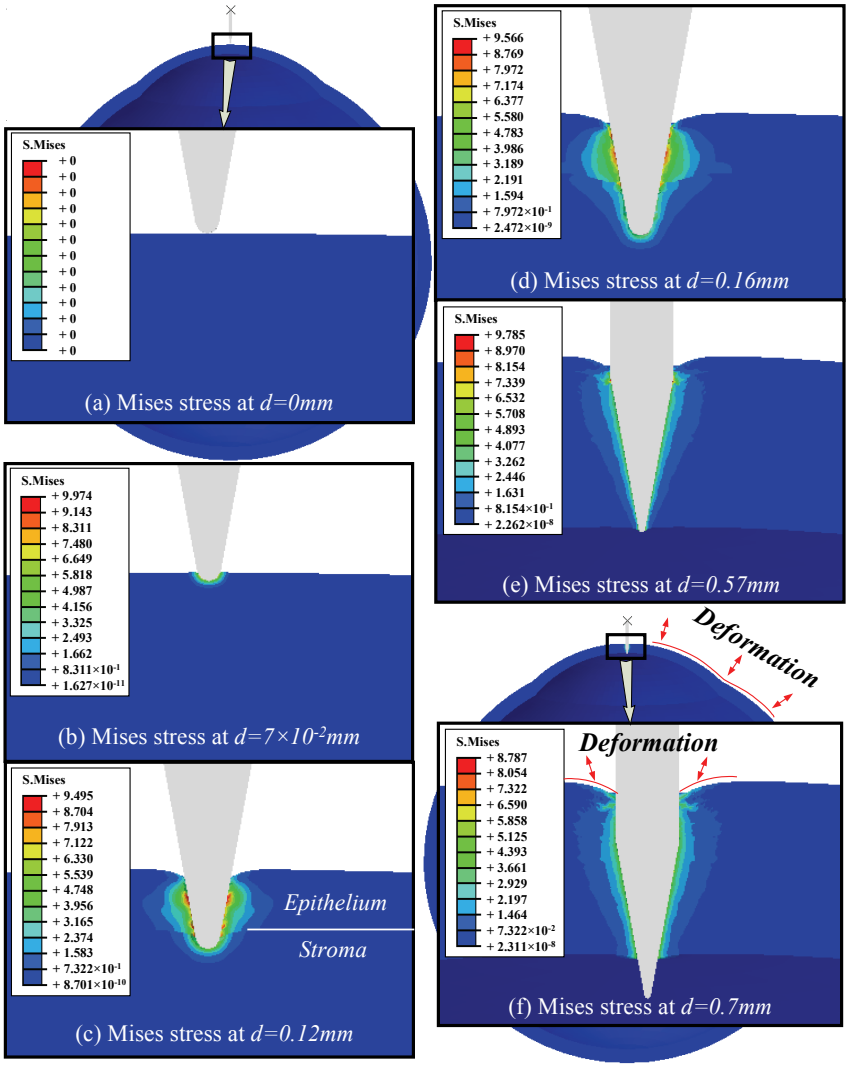

Fig. 10. Maps of von Mises stress for insertion simulation when insertion speed is 1 mm/s, where d is insertion depth. (a) corneal pre-deformed status; (b) corneal epithelium has been punctured; (c) the stroma has been punctured; (d) punctured status of stroma at d = 0.16 mm; (e) the lower surface of the cornea has been punctured; (f) broken status of the cornea at d = 0.7 mm

4. Discussion

The process of needle insertion into cornea is a complex nonlinear problem including material nonlinearity, geometric nonlinearity and boundary nonlinearity. In the process, the insertion force, an important parameter, would be generated owing to the interactions between rigid body and viscoelastic object, which could be used to determine insertion depth. Although the force has been measured in previous reports [21], [31], biomechanical simulation of the process has not achieved the desired results due to the complexity.

Many scholars have done a lot of works in measurement of corneal biomechanical properties, but the properties of cornea are different under different physiological conditions or test specifications [10]. The previous study describes a corneal constitutive model that is a relatively simple material model including hyperelastic and viscoelastic ones [26]. It is important to ensure the authenticity and validity of insertion simulation. Material parameters of the model, obtained by uniaxial tensile test and stress relaxation test, are broadly in line with the results of previous publication, even though there are some differences in the accurate results due to different testing conditions.

Although some scholars had studied microscopic structure of the cornea [3], few distinguished structural layer during insertion simulation of the cornea. In this paper, the cornea is divided into two structural layers including epithelium and stroma according to corneal structures and biomechanical properties. The idea to distinguish structural layer is the first to be applied to insertion simulation of the cornea. As a cell-based membrane, epithelium is believed to offer a larger hardness to needle puncture. The cornea is confined by external tissues, which contribute to the internal stress and to the actual configuration of the cornea, where there is close association between cornea and sclera, and they together constitute the outer wall of the eye. On this basis, corneal constraint is considered in finite element model.

Insertion force-displacement curves are obtained based on experiment of needle insertion into cornea. Analyzing the curves, we found that the force is nonlinearly increasing with the insertion depth before the cornea was punctured completely, and there is fluctuation of force caused by tissue deformation. When the eyeball is extracted from the body, the confinement disappears and this leads to an "expansion" of the eyeball because a confinement is missing, and the IOP is reduced correspondingly. Although it cannot compensate the expansion of the eye, IOP value is to maintain the ideal value (i.e., 17.5 mmHg) by injecting saline to the eyeball in order to ensure the consistency and remove experimental variability in the mechanical response.

Finally, applying the distortion energy failure criterion of corneal material, the process of needle insertion into cornea is simulated in ABAQUS. According to the relationship between the insertion force and depth, obtained by simulation, we could find that the larger insertion speed tends to increase insertion force and decrease fluctuation of the force. Although the simulation describes the biomechanical behavior in ideal conditions, the correctness of the simulation is verified by comparisons with the experimental results.

Admittedly, there are some limits and drawbacks about the approach. For example, the paper studies the insertion force, but it can be subdivided as a summation of stiffness, friction, and cutting forces to obtain more accurate results [21]. The final structural model of the corneal shell which is a simplification is in discord with the theoretically advanced description, so a more accurate model with the physical nonlinearity should be built as the technology improves. Besides, porcine corneas are taken as the test subjects due to the difficulty in obtaining human ones, but they cannot completely substitute human ones because of different mechanical behaviors [6], [11].

We are evaluating the possibility of performing the surgery of robot-assisted corneal suturing based on the results from this study. With further biomechanical research we will explore the indicators of the force feedback which can be used to determine the progress of robot-assisted surgery, and explore the ways to implement real-time simulation of corneal suture surgery combining robotics and finite element methods.

Acknowledgement

The author wishes to thank the Natural Science Foundation of China (Grant No. 50675008 and Grant No. 51175013) that supported this work.

References

[1] ABOLHASSANI N., PATEL R., MOALLEM M., *Needle insertion into soft tissue: A survey*, Med. Eeg. Phys., 2007, 29(4), 413–431.

[2] ALTMAN D.A., HOETZEL D.A., BUZARD K., CHOE K., *Strip extensiometry for comparison of the mechanical response of bovine, rabbit and human corneas*, J. Biomech. Eng., 1992, 114(2), 202–215.

[3] ANDERSON K., EL-SHEIKH A., NEWSON T., *Application of structural analysis to the mechanical behaviour of the cornea*, J. R. Soc. Interface, 2004, 1(1), 3–15.

[4] BERKLEY J., TURKIYYAH G., BERG D., GANTER M., WEGHORST S., *Real-time finite element modeling for surgery simulation: An application to virtual suturing*, IEEE T. Vis. Comput. Gr., 2004, 10(3), 314–325.

[5] BISPLINGHOFF J.A., MC-NALLY C., MANOOGIAN S.J., DUMA S.M., *Dynamic material properties of the human sclera*, J. Biomech., 2009, 42(10), 1493–1497.

[6] BOSCHETTI F., TRIACCA V., SPINELLI L., PANDOLFI A.. *Mechanical characterization of porcine corneas*, J. Biomech. Eng., 2012, 134(3), 031003.

[7] DAVIS S.P., LANDIS B.J., ADAMS Z.H., ALLEN M.G., *Prausnitz MR. Insertion of microneedles into skin: measurement and prediction of insertion force and needle fracture force*, J. Biomech., 2004, 37, 1155–1163.

[8] DIMAIO S.P., SALCUDEAN S.E., *Needle insertion modeling and simulation*, IEEE Trans. Robot. and Autom., 2003, 19(5), 864–875.

[9] EHLERS N., HJORTDAL J., *Corneal thickness: measurement and implications*, Exp. Eye. Res., 2004, 78(3), 543–548.

[10] ELSHEIKH A., ALHASSO D., RAMA P., *Biomechanical properties of human and porcine corneas*, Exp. Eye. Res., 2008, 86(5), 783–790.

[11] ELSHEIKH A., KASSEM W., JONES S.W., *Strain-rate sensitivity of porcine and ovine corneas*, Acta Bioeng. Biomech., 2011, 13(2), 25–36.

[12] FANG X., XU Y., *Corneal stress-strain relation and structural equation of porcine eye after LASIK*, Int. J. Ophthalmol., 2006, 6(6).

[13] FRATZL P., MISOF K., ZIZAK I., RAPP G., AMENITSCH H., BERNSTORFF S., *Fibrillar structure and mechanical properties of collagen*, J. Struct. Biol., 1998, 122(1), 119–122.

[14] GERE J.M., GOODNO B.J., *Mechanics of Materials*, Cengage Learning, 2009.

[15] GENT A.N., *Engineering with rubber: how to design rubber components*, Carl Hanser Verlag GmbH Co., KG, 2012.

[16] HATAMI-MARBINI H., *Viscoelastic shear properties of the corneal stroma*, J. Biomech., 2014, 47(3), 723–728.

[17] HOLZAPFEL G.A., *Nonlinear solid mechanics*, Chichester, Wiley, 2000.

[18] JONES R.M., *Mechanics of composite materials*, CRC Press, 1998.

[19] LI L., TIGHE B., *The anisotropic material constitutive models for the human cornea*, J. Struct. Biol., 2006, 153(3), 223–230.

[20] MARSHALL P., PAYANDEH S., DILL J., *Suturing for surface meshes*, CCA, 2005, 31–36.

[21] OKAMURA A.M., SIMONE C., O'LEARY M.D., *Force modeling for needle insertion into soft tissue*. IEEE Trans. Biomed. Eng., 2004, 51(10), 1707–1716.

[22] PANDOLFI A., MANGANIELLO F., *A model for the human cornea: constitutive formulation and numerical analysis*, Biomech. Model. Mechan., 2006, 5(4), 237–246.

[23] ROESTHUIS R.J., VAN-VEEN Y.R., JAHYA A., MISRA S., *Mechanics of needle-tissue interaction*, IROS, 2011, 2557–2563.

[24] STITZEL J.D., DUMA S.M., CORMIER J.M., HERRING I.P., *A nonlinear finite element model of the eye with experimental validation for the prediction of globe rupture*, Stapp car Crash Journal, 2002, 46, 81–102.

[25] STUDER H.P., RIEDWYL H., AMSTUTZ C.A., HANSON J.V., BUCHLER P., *Patient-specific finite-element simulation of the human cornea: A clinical validation study on cataract surgery*, J. Biomech., 2013, 46(4), 751–758.

[26] SU P., YANG Y., XIAO J., SONG Y., *Corneal Hyperviscoelastic Model: Derivations, Experiments, and Simulations*, Acta Bioeng. Biomech., 2015, 17(2), 73–84.

[27] VAN-GERWEN D.J., DANKELMAN J., VAN-DEN-DOBBELSTEEN J.J., *Needle–tissue interaction forces – A survey of experimental data*, Med. Eng. Phys., 2012, 34(6), 665–680.

[28] XUAN X., YANG Y., WANG Z., DENG S., LIU X., *Force modeling for needle insertion into corneal tissue*, Chinese High Technology Letters, 2009, (9), 951–956.

[29] YAN J., STRENKOWSKI J.S., *A finite element analysis of orthogonal rubber cutting*, J. Mater. Process. Tech., 2006, 174(1), 102–108.

[30] YANG Y., LIU X., FU H., *Finite Element Simulation of Needle Insertion into Cornea*, Chin. J. Mech. Eng., 2008, 44(12), 24–29.

[31] YANG Y., XU C., DENG S., XIAO J., *Insertion force in manual and robotic corneal suturing*, Int. J. Med. Robot. Comp., 2012, 8(1), 25–33.